Piezoelectric Shunt Stiffness in Rhombic Piezoelectric Stack Transducer with Hybrid Negative-Impedance Shunts: Theoretical Modeling and Stability Analysis

Leiying He [1] [iD] **, Wenguang Zheng** [1,2,*] **, Chenxue Zhao** [1] **and Chuanyu Wu** [1,*]

1   Faculty of Mechanical Engineering & Automation, Zhejiang Sci-Tech University, Hangzhou 310018, China
2   School of Mechanical Engineering & Automation, University of Science and Technology Liaoning, Anshan 114051, China
*   Correspondence: zhengwg@ustl.edu.cn (W.Z.); cywu@zstu.edu.cn (C.W.)

check for
updates

Abstract: Negative-capacitance shunted piezoelectric polymer was investigated in depth due to its considerable damping effect. This paper discusses the novel controlled stiffness performance from a rhombic piezoelectric stack transducer with three hybrid negative-impedance shunts, namely, negative capacitance in series with resistance, negative capacitance in parallel with resistance, and negative inductance/negative capacitance (NINC) in series with resistance. An analytical framework for establishing the model of the coupled system is presented. Piezoelectric shunt stiffness (PSS) and piezoelectric shunt damping (PSD) are proposed to analyze the stiffness and damping performances of the hybrid shunts. Theoretical analysis proves that the PSS can produce both positive and negative stiffness by changing the negative capacitance and adjustable resistance. The Routh–Hurwitz criterion and the root locus method are utilized to judge the stability of the three hybrid shunts. The results point out that the negative capacitance should be selected carefully to sustain the stability and to achieve the negative stiffness effect of the transducer. Furthermore, negative capacitance in parallel with resistance has a considerably better stiffness bandwidth and damping performance than the other two shunts. This study demonstrates a novel electrically controlled stiffness method for vibration control engineering.

Keywords: controlled stiffness; negative capacitance; shunt damping; vibration control; piezoelectric

1. Introduction

Piezoelectric transducers are widely used for vibration control [1–3], energy harvesting [4–8], health monitoring [9,10], and sensing. Piezoelectric shunt damping involves the connection of an electrical impedance to terminals of a piezoelectric transducer (PZT), and it was widely studied since Forward carried out a preliminary experimental demonstration of the feasibility of using external electronic circuits to control mechanical vibrations in optical systems [11]. Hagood and von Flotow [12] studied a resistive shunt that is able to dissipate vibrational energy in the form of heat. A piezoelectric patch that consists of a single resonant circuit with an inductor can generate electrical resonance to reduce vibration [13–15]. The passive multimode resonant shunts, such as the Hollkamp shunt [16], the current-blocking shunt [17], the current-flowing shunt [18], and the series–parallel shunt [19], were investigated to control multimodal vibrations of host structures. These resonant shunts were applied to control the vibration of a compact disc read-only memory (CD-ROM) [20], a hard disk drive (HDD) disk–spindle system [21–23], a smart panel [24], a uniform bimorph beam (simulating chatter) [25], etc. The closed-form solution [26], H∞ [27], matrix inequalities [28], and equal modal damping [29] were employed to optimize the shunt parameters. The pure passive resistive shunt offers

a little damping to the mechatronic system. The resonant shunt works like a tuned mass damper that is sensitive to the change in natural frequency [30]. To overcome these two drawbacks of the passive shunt, adaptive multimode resonant shunts were proposed to adjust the change in frequency so as to achieve considerable vibration control [31].

Compared to those shunts that only use passive electronics, such as a resistor, a capacitor, and an inductor, the active shunt needs an external electrical energy to drive it, such as operational amplifiers, transistors, and electronic switches [2,3,32,33]. Fleming et al. [34] used the active Linear-Quadratic-Gaussian (LQG), H2, and H∞ methods to optimize a suitable impedance of the shunt. The piezoelectric transducer can be electrically simplified to a capacitance and a current source. The negative capacitance is able to cancel the inherent capacitance of the piezoelectric transducer so as to realize broadband vibration control [35]. The negative capacitance can be constructed by a negative impedance converter (NIC) that can also be used to construct negative resistance [36–39] and negative inductance [40]. Neubauer et al. [41] studied the effect of negative-capacitance shunted piezoelectric transducers in absorbing systems. Manzoni et al. [42] discussed the values of the electric elements composing the negative capacitance to improve vibration reduction efficiency and to avoid instability at low frequencies. Beck et al. [43] suggested that the negative-capacitance shunt can modify the effective modulus of the piezoelectric transducer, and discussed the power output and efficiency of negative capacitance. Han et al. [44] proposed an adaptive shunt that consists of a switched inductance/resistance in parallel with negative capacitance to improve damping performance. Neubauer et al. [45] used it to control the vibration of a bladed disc. Gripp et al. [46] described an adaptive resonant piezoelectric vibration absorber enhanced by synthetic negative capacitance. The resonant shunt circuit autonomously adapted the inductance value by comparing the phase difference of the vibration velocity and the current flowing through the shunt. Synthetic negative capacitance was employed to enhance the vibration attenuation performance. Pohl et al. [47] studied an adaptive negative-capacitance circuit to improve the robustness of PSD, and to improve the performance of the negative-capacitance shunt by enlarging the output voltage to the requirements of piezoelectric transducers. The other studies and applications on negative-capacitance shunts can be found in Reference [48].

The existing research efforts mainly focused on how to use negative-capacitance shunted piezoelectric patches to suppress structural vibrations [49,50]. Preumont [51] and Marneffe [1] began applying the negative-capacitance shunted piezoelectric stack to the vibration control of a truss structure. Manzoni et al. [42] and Beck et al. [43] showed that a carefully chosen negative capacitance can produce a change in stiffness and the frequency shift phenomenon. Heuss [52] discussed tuning of a vibration absorber with negative-capacitance shunted piezoelectric patches. That is the first time the value of negative capacitance used was bigger than the inherent capacitance of a transducer. These studies mainly discussed the damping performance of PSD.

Up to now, few studies considered the stiffness effect of negative-capacitance shunted PSD. Zheng et al. [53] discussed the tuning of natural frequency with an electromagnetic shunt mass. Consequently, this study focuses on the stiffness mechanism of PSD, and discusses the use of the negative stiffness to enhance the structural vibration isolation performance. The aim of the study is different from the previous studies [49–52]. The theoretical model of the coupled electromechanical system is obtained according to Lagrange's equation. The piezoelectric shunt stiffness is proposed and analyzed. The stability of the transducer is theoretically analyzed according to the Routh–Hurwitz criterion and graphically discussed with the root locus method. The damping and stiffness effects are also discussed.

2. Materials and Methods

2.1. Modeling of the Rhombic Piezoelectric Stack Transducer

Figure 1 shows a rhombic piezoelectric stack transducer with a hybrid negative-impedance shunt circuit. Compared to positive impedance, the equivalent value of the negative impedance is

negative. The rhombic frame can magnify the output displacement of the piezoelectric transducer like an operation amplifier; the corresponding amplification coefficient can be found in Reference [54]. The terminals of the piezoelectric stack transducer connect to a hybrid NIC shunt, which consists of an adjustable impedance Z_a and an NIC. The NIC is constructed by an operational amplifier [1,35,55]. The input impedance of the circuit created by the passive impedances Z_1, Z_2, and Z_s is $Z = -\frac{Z_1}{Z_2}Z_s$ [43]. If $Z_1 = Z_2$, the equivalent impedance of the operational amplifier will be $-Z_s$. When Z_s is replaced with a capacitor, an inductor, or a resistor, we can obtain equivalent negative capacitance, negative inductance, or negative resistance. In the present study, we discuss the effect of negative capacitance on the stiffness performance of PSD. It should be noted that the rhombic frame is used to install the stack. In general, the stiffness of the rhombic frame is very big; thus, it should be carefully designed for vibration isolation application.
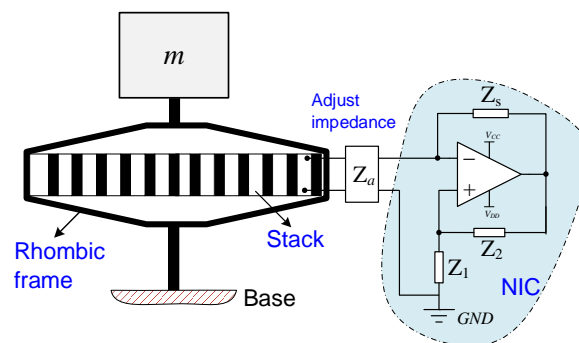

Figure 1. Model of a rhombic piezoelectric stack transducer with a hybrid negative-impedance shunt circuit. Z_a is the adjustable impedance of shunt; it can be in series and parallel forms. Z_1, Z_2, and Z_s are utilized to construct the different types of shunt.

Figure 2a is the electrical equivalent model of the piezoelectric stack transducer with the hybrid shunt. The governing equation of the rhombic piezoelectric stack transducer with the hybrid negative-impedance shunt is modeled with Lagrange's equation,

$$\frac{d}{dt}\left(\frac{\partial L}{\partial \dot{q}_i}\right) - \frac{\partial L}{\partial q_i} = Q_i, \tag{1}$$

where $L = T + W - U$ is the Lagrangian of the system, and Q_i is the nonconservative force associated with the generalized coordinates. T is the kinetic energy of the piezoelectric transducer,

$$T = \frac{1}{2}\dot{x}^T m \dot{x}. \tag{2}$$

U is the restored deformation energy of the rhombic frame,

$$U = \frac{1}{2}x^T k x, \tag{3}$$

where k is the stiffness of the rhombic frame.

W is the energy of the piezoelectric stack transducer,

$$W = \frac{1}{2}C_P V^2 + n d_{33}K_a V x - \frac{1}{2}K_a x^2, \tag{4}$$

where $C_p = C(1 - k_p^2)$ is the capacitance of the transducer under constant extension, and the electromechanical coupling factor of the transducer k_p^2 is the efficiency of the conversion of mechanical energy into electricity, which ranges around 0.5 for PZT [1]. The stack includes n discs. The stiffness with short-circuited electrodes is K_a, and d_{33} is the piezoelectric constant. V is the voltage between the

electrodes. Figure 2b is the equivalent model of hybrid shunts. The nonconservative virtual work is related to the damping of the rhombic frame. The dissipated work through the shunt circuit and the external excitation force is as follows:

$$\delta W_{nc} = -c\dot{x}\delta x - I_s\delta V + F\delta x. \tag{5}$$

Substituting Equations (2)–(5) into Equation (1), the governing equations of the coupled electromechanical system are as follows:

$$m\ddot{x} + c\dot{x} + (k + K_a)x - \theta V = F, \tag{6}$$

$$C_P\dot{V} + \theta\dot{x} + I_s = 0, \tag{7}$$

where $\theta = nd_{33}K_a$ is the electromechanical coupling coefficient of the stack, and I_s is the current flowing in the circuit. The structural damping coefficient c is represented by $c = 2\zeta\omega_n/m$, and the structural damping ratio ζ can be selected between 0.5% and 1%. The natural frequency ω_n is represented by $\sqrt{(k + K_a)/m}$.
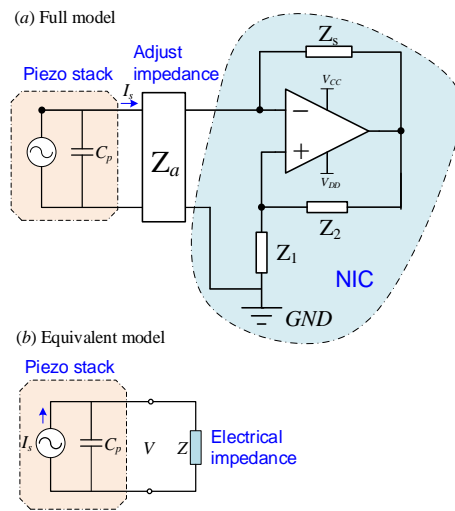

Figure 2. Electrical model of the piezoelectric stack transducer with the hybrid shunt: (**a**) full schematic, and (**b**) equivalent impedance model.

2.2. Concept of Controlled Stiffness with Hybrid Negative-Impedance Shunts

2.2.1. Model for the Negative-Impedance Shunt

In the time domain, Equations (6) and (7) cannot reflect the stiffness effect of the hybrid shunt. In the Fourier domain, these two equations are as follows:

$$-\left[(k + K_a) - m\omega^2 + jc\omega\right]x - \theta V = F, \tag{8}$$

$$j\omega C_P V + j\theta\omega x + I_s = 0. \tag{9}$$

If the shunt is represented by an equivalent impedance Z shown in Figure 2b, we have $I_s = V/Z$. Then, Equation (9) becomes

$$V = \frac{-j\omega\theta}{j\omega C_p + 1/Z}x. \tag{10}$$

Substituting Equation (10) into Equation (8), the transfer function is as follows:

$$\frac{x}{F} = \frac{1}{(k + K_a) - m\omega^2 + j\omega(c + c_{sh})}, \tag{11}$$

$$c_{sh} = \frac{\theta^2}{j\omega C_p + 1/Z}.\tag{12}$$

It can be found that the shunt brings the damping into the piezoelectric stack transducer, which can possibly reduce structural vibration. If Equation (12) is written as

$$c_{sh} = \frac{1 - j\omega Z C_p}{1 + \omega^2 Z^2 C_p^2}\theta^2 Z,\tag{13}$$

then Equation (11) is reorganized as

$$\frac{x}{F} = \frac{1}{(k + K_a) - (m + m_s)\omega^2 + j\omega(c + c_s)},\tag{14}$$

$$m_s = \frac{-\theta^2 Z^2 C_p}{1 + \omega^2 Z^2 C_p^2},\tag{15}$$

$$c_s = \frac{\theta^2 Z}{1 + \omega^2 Z^2 C_p^2}.\tag{16}$$

These three equations imply that the introducing of a shunt circuit brings both the damping and the mass effects into the transducer, where m_s and c_s are defined as the piezoelectric shunt mass (PSM) and piezoelectric shunt damping, respectively. The variation of the mass and stiffness influences the natural frequency of the transducer. Therefore, Equation (14) can also be reorganized as

$$\frac{x}{F} = \frac{1}{(k + K_a + k_s) - m\omega^2 + j\omega(c + c_s)},\tag{17}$$

$$k_s = \frac{\omega^2 \theta^2 Z^2 C_p}{1 + \omega^2 Z^2 C_p^2},\tag{18}$$

where k_s is defined as the piezoelectric shunt stiffness. Equation (18) suggests that the PSS is associated with the excitation frequency, the adjustable impedance, and the capacitance of the shunt circuit.

Figure 3 presents the positive and negative capacitance at the complex plane. The horizontal axis represents the resistance, and the vertical axis represents the capacitance. The controlled PSS will be different upon changing the shunt impedance in different quadrants. The negative capacitance $-1/jc\omega$ can be rewritten as $j/c\omega$; it is somewhat like the positive inductance, but the frequency relationship is reciprocal. In previous studies [42,51], the negative capacitance was laid at the first quadrant. In this study, we move the impedance location of the shunt to the second quadrant, and discuss the stiffness and damping effects by changing the value of the negative capacitance.
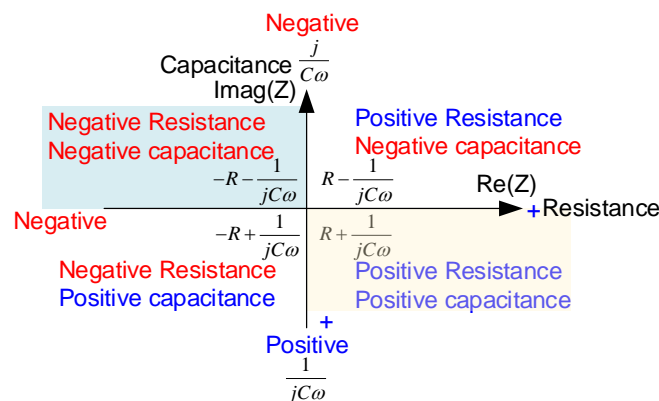

Figure 3. Complex plot of capacitance considering both the positive and negative cases.

2.2.2. Negative Capacitance in Series with Resistance

A resistor R connected in series with a capacitor C_s can increase the leakage of the negative resistance, as shown in Figure 4a. R is necessary and should be large enough due to the bias currents flowing from the non-ideal operational amplifier. The parallel resistor and capacitor act like a high-pass filter allowing bias current to flow to ground, thus preventing the capacitor from acquiring a direct current (DC) charge [35]. The equivalent impedance of the NIC circuit is

$$Z_s = -\Gamma_R \frac{1}{1/R + j\omega C_s},\tag{19}$$

where $\Gamma_R = R_1/R_2$. Assuming that $\Gamma_R = 1$ and taking the adjustable resistor R_s into consideration, the total impedance of this series shunt is

$$Z = R_s - \frac{1}{1/R + j\omega C_s}.\tag{20}$$

If this hybrid shunt connects to the piezoelectric stack transducer, then Equation (15) becomes

$$c_{sh} = c_s - j\frac{k_s}{\omega}.\tag{21}$$

This equation shows the relationship between the PSS and PSD. The coefficients c_s and k_s are as follows:

$$c_s = \theta^2 \frac{\left(1/R - \omega^2 R_s C_s C_p\right)(R_s/R - 1) + \left(C_s - C_p + R_s C_p/R\right)\omega^2 R_s C_s}{\left(1/R - \omega^2 R_s C_s C_p\right)^2 + \left(C_s - C_p + R_s C_p/R\right)^2 \omega^2},\tag{22}$$

$$k_s = -\frac{\theta^2 \omega^2 \left[R_s C_s\left(1/R - \omega^2 R_s C_s C_p\right) - (R_s/R - 1)\left(C_s - C_p + R_s C_p/R\right)\right]}{\left(1/R - \omega^2 R_s C_s C_p\right)^2 + \left(C_s - C_p + R_s C_p/R\right)^2 \omega^2}.\tag{23}$$
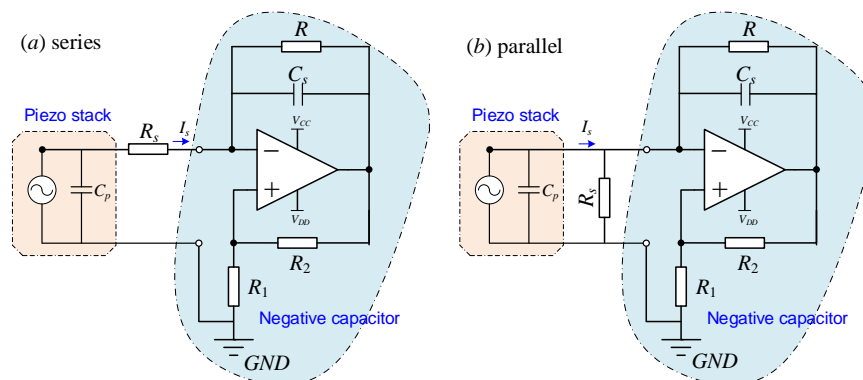

Figure 4. Piezoelectric stack transducer with negative capacitance and adjustable resistance R_s: (**a**) in series and (**b**) in parallel. The resistor R is utilized to increase the leakage of the capacitor C_s.

2.2.3. Negative Capacitance in Parallel with Resistance

Figure 4b is the schematic of the negative capacitance in parallel with R_s, where the total impedance of the shunt is

$$Z = \frac{1}{1/R_s - (1/R + j\omega C_s)}.\tag{24}$$

Substituting into Equation (21) and simplifying it, we can obtain c_s and k_s.

$$c_s = \frac{\theta^2(1/R_s - 1/R)}{(1/R_s - 1/R)^2 + \omega^2\left(C_p - C_s\right)^2}, \tag{25}$$

$$k_s = \frac{\theta^2\omega^2\left(C_p - C_s\right)}{(1/R_s - 1/R)^2 + \omega^2\left(C_p - C_s\right)^2}. \tag{26}$$

2.2.4. Negative Inductance and Negative Capacitance in Series with Resistance

If the equivalent impedance Z_s in Figure 2a is replaced by an inductor L_s and a capacitor C_s in series, and Z_1 and Z_2 are resistors, the schematic is as presented in Figure 5. Assuming that R_1 is equal to R_2, then the impedance of the NIC is

$$Z_s = -\Gamma_R\left(j\omega L_s + \frac{1}{j\omega C_s}\right). \tag{27}$$

Thus,

$$Z = R_s - \Gamma_R\left(j\omega L_s + \frac{1}{j\omega C_s}\right). \tag{28}$$

Substituting Equation (28) into Equation (12), one can obtain

$$c_s = \theta^2\frac{R_sC_sC_p\Gamma_R\left(1 - \omega^2L_sC_s\right) + R_sC_s\left\{C_s - C_p\left[\Gamma_R\left(1 - \omega^2L_sC_s\right)\right]\right\}}{\left(\omega R_sC_sC_p\right)^2 + \left\{C_s - C_p[\Gamma_R(1 - \omega^2L_sC_s)]\right\}^2}, \tag{29}$$

$$k_s = -\frac{\theta^2\left[\left\{C_s - C_p\left[\Gamma_R\left(1 - \omega^2L_sC_s\right)\right]\right\}\Gamma_R\left(1 - \omega^2L_sC_s\right) - \omega^2R_s^2C_s^2C_p\right]}{\left(\omega R_sC_sC_p\right)^2 + \left\{C_s - C_p[\Gamma_R(1 - \omega^2L_sC_s)]\right\}^2}. \tag{30}$$
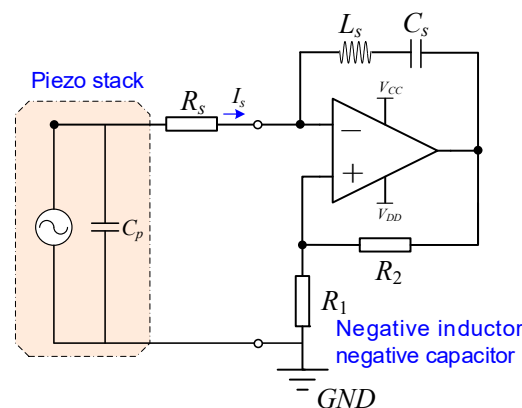

Figure 5. Schematic of the piezoelectric stack transducer with the negative inductance/negative capacitance (NINC) in series with the resistance shunt circuit.

3. Results

3.1. Analysis of the PSS for the Three Hybrid Shunts

We already obtained the PSS k_s for the three hybrid shunts. The influence of PSD on PSS is quite important, which determines the design of the controlled stiffness transducer. If k_s is divided by c_s,

$$\kappa_c = \frac{k_s}{c_s}, \tag{31}$$

κ_c is defined as the stiffness and damping ratio of the PSD.

For the negative capacitance in series with the resistance shunt case, according to Equation (31),

$$\kappa_c = -\omega^2 \frac{R_sC_s\left(1/R - \omega^2 R_s C_s C_p\right) - (R_s/R - 1)\left(C_s - C_p + R_s C_p/R\right)}{\left(1/R - \omega^2 R_s C_s C_p\right)(R_s/R - 1) + \left(C_s - C_p + R_s C_p/R\right)\omega^2 R_s C_s}. \tag{32}$$

For the negative capacitance in parallel with the positive resistance shunt case,

$$\kappa_c = \omega^2 \frac{C_p - C_s}{1/R_s - 1/R}. \tag{33}$$

For the negative inductance and negative capacitance in series with resistance case,

$$\kappa_c = \frac{\left\{C_s - C_p\left[\Gamma_R\left(1 - \omega^2 L_s C_s\right)\right]\right\}\Gamma_R\left(1 - \omega^2 L_s C_s\right) - \omega^2 R_s^2 C_s^2 C_p}{R_s C_s C_p \Gamma_R (1 - \omega^2 L_s C_s) + R_s C_s\left\{C_s - C_p[\Gamma_R(1 - \omega^2 L_s C_s)]\right\}}. \tag{34}$$

Table 1 lists the parameters of the piezoelectric stack transducer and the hybrid shunts that are obtained from the experiment. According to the theoretical model of the PSS and PSD obtained in Section 3, the stiffness performance of the hybrid shunts is discussed below.

Table 1. Parameters of the piezoelectric stack and the hybrid shunts.

Parameters (Unit)	Value
Piezoelectric charge coefficient, d_{33} (C/N)	400×10^{-12}
Capacitance of the stack, C_p (µF)	1.478
R (Ω)	1×10^6
T_R	1
L_s (mH)	10
Mass, m (kg)	0.1
Natural frequency of transducer, f_n (Hz)	154.9

Figure 6 shows the variation of the natural frequency f_n, k_s, c_s, and κ_c with respect to the adjustable resistance R_s for the negative capacitance in series with R_s shunt. When C_s is −0.6 µF, the changes of f_n and k_s are very small, which means that it is hard to generate the electrically controlled stiffness effect. The corresponding damping effect is also small. When the negative capacitance is −1 µF, f_n and k_s increase. When the negative capacitance increases to −1.4 µF, which means that the absolute value of negative capacitance approximates to the inherent capacitance of the piezoelectric stack C_p, then f_n and PSS begin to change in a very large range. The stiffness is a positive value that increases the natural frequency of the transducer. In this case, the damping effect changes with the change of R_s, and it can easily find an optimal value. When the negative capacitance is further increased to −2 µF, which means C_s is bigger than C_p, f_n also decreases apparently. In this case, the PSS produces the negative stiffness effect that decreases with the increase of R_s. The corresponding damping effect is within an acceptable range.

Figure 7 is the variation of the natural frequency f_n, k_s, c_s, and κ_c with respect to the adjustable resistance R_s for the negative capacitance in parallel with resistance shunt. The negative capacitance for −0.6 µF, −1 µF, −1.4 µF, and −2 µF cases is discussed. When the negative capacitance is increased from −0.6 µF to −1.4 µF, k_s is positive, increasing the natural frequency of the transducer, and the natural frequency also increases with the increase of the negative capacitance. The damping performance is excellent when the negative capacitance is −1.4 µF. When the negative capacitance is further increased to −2 µF, f_n decreases dramatically. In this case, the PSS produces the negative stiffness effect that decreases with the increase of R_s.
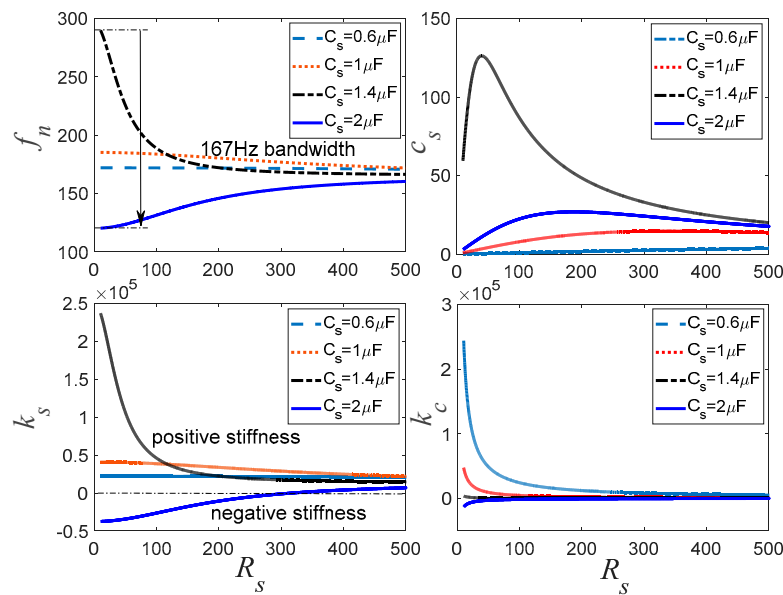
Figure 6. Controlled stiffness analysis for the negative capacitance in series with R_s shunt.
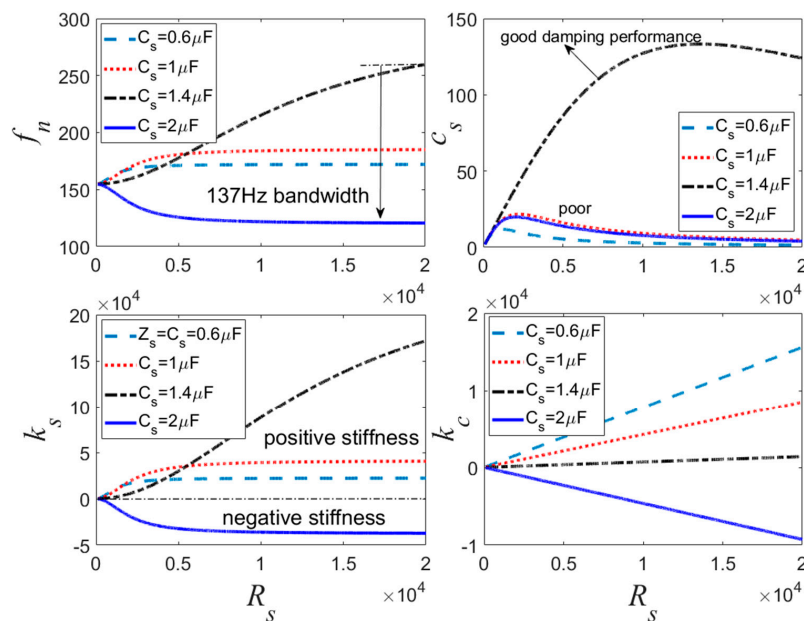

Figure 7. Controlled stiffness analysis for the negative capacitance in parallel with R_s shunt.

Figure 8 is the variation of the natural frequency, PSS, PSD, and κ_c with respect to the resistance R_s for the negative inductance/negative capacitance in series with resistance shunt. When the negative capacitance is -1 μF, the changes of f_n and k_s are small, and the c_s is also small, making it hard to control the vibration of the system. When the negative capacitance increases to -1.4 μF, f_n and k_s begin to change in a very large range. k_s is positive, increasing the natural frequency of the transducer. The PSD c_s increases apparently and the optimal c_s appears when R_s is 165.2 Ω. When the negative capacitance is further increased to -2 μF, f_n also decreases like the other two kinds of shunts; k_s is also a negative stiffness.

Figures 6–8 also imply that κ_c is very big when c_s is small. When c_s increases, κ_c tends to a small value. This demonstrates that κ_c can be used for evaluating the damping effect of the PSD. If we combine f_n and k_s curves shown in Figures 6–8 together, it can be found that the negative capacitance in parallel with resistance case has a relative stable controlled natural frequency and better stiffness performance compared to the other two hybrid shunts. With this hybrid shunt, κ_c curves are straight lines. When the

absolute value of negative capacitance is bigger than C_p, the controlled stiffness may be negative, which results in the decrease of the natural frequency of the transducer. Conversely, when the absolute value of negative capacitance is smaller than C_p, the controlled stiffness is positive, which increases the natural frequency of the transducer. k_s increases with the increase of the negative capacitance of the shunt. The natural frequency is determined mostly by the negative capacitance, and the PSS c_s is determined by R_s. However, when the absolute value of the negative capacitance approximates to C_p, R_s dramatically influences k_s. Consequently, the negative capacitance and the adjustable resistance should be carefully selected to sustain considerable stiffness and damping performance.
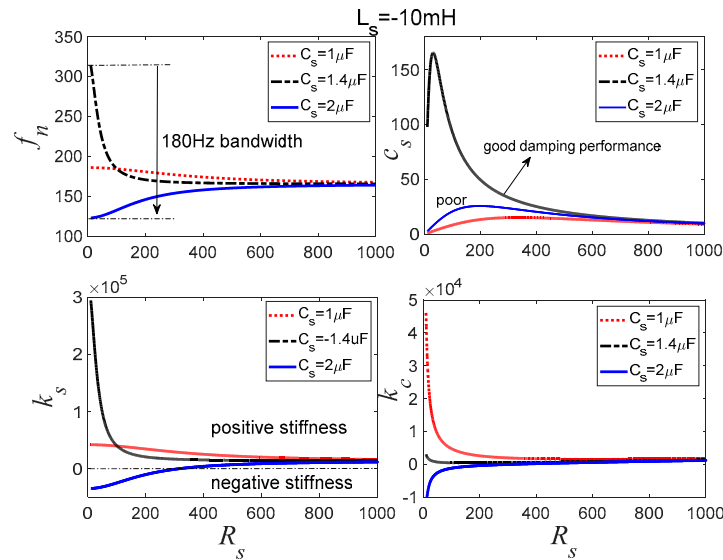

Figure 8. Controlled stiffness analysis for the negative inductance/negative capacitance in series with R_s shunt.

3.2. Stability Analysis

3.2.1. Routh–Hurwitz Criterion

1. Negative capacitance in series with resistance

Note that when $s = j\omega$, $\omega_n^2 = (k + K_a)/m$, then the characteristic function of the piezoelectric stack transducer with the hybrid shunts can be obtained according to Equation (11),

$$s^2 + \frac{c + c_{sh}}{m}s + \omega_n^2 = 0. \tag{35}$$

For the negative capacitance in series with resistance shunt, when $R \to \infty$, then

$$c_{sh} = \frac{\theta^2(sR_sC_s - 1)}{s^2R_sC_sC_p - s(C_p - C_s)}. \tag{36}$$

The inherent capacitance of the piezoelectric stack C_p and the negative capacitance C_s are all in the microfarad scale; thus, $C_s C_p$ can be neglected to some extent, and the characteristic function of the closed-loop system is as follows:

$$(C_p - C_s)s^2 + \left[2\varsigma\omega_n(C_p - C_s) - \theta^2R_sC_s/m\right]s + \left[\theta^2/m + \omega_n^2(C_p - C_s)\right] = 0. \tag{37}$$

The Routh array is

$$
\begin{array}{c|cc}
s^2 & C_p - C_s & \theta^2/m + \omega_n^2\left(C_p - C_s\right) \\
s^1 & 2\varsigma\omega_n\left(C_p - C_s\right) - \theta^2 R_s C_s/m & 0 \\
s^0 & \theta^2/m + \omega_n^2\left(C_p - C_s\right) & 0
\end{array}
\tag{38}
$$

The necessary and sufficient condition for the stability of this system is that the first column of the Routh array in Equation (38) is positive.

When $C_p > C_s$, the following relationship is required to keep the stability of the control system:

$$
2\varsigma\omega_n\left(C_p - C_s\right) - \theta^2 R_s C_s/m > 0; \theta^2/m + \omega_n^2\left(C_p - C_s\right) > 0.
\tag{39}
$$

Then, one can get

$$
C_s < \min\left\{\frac{C_p}{1 + \theta^2 R_s/(2\varsigma m\omega_n)}, C_p + \frac{\theta^2}{m\omega_n^2}\right\}.
\tag{40}
$$

The abovementioned equation suggests that

$$
\frac{C_p}{1 + \theta^2 R_s/(2\varsigma m\omega_n)} < C_p < \frac{\theta^2}{m\omega_n^2} + C_p.
\tag{41}
$$

Thus, C_s should be selected as

$$
C_s < \frac{C_p}{1 + \theta^2 R_s/(2\varsigma m\omega_n)}.
\tag{42}
$$

When $C_p < C_s$, the capacitance of the circuit is negative; with the same process, the following condition should be met:

$$
C_s > \max\left\{\frac{2\varsigma\omega_n C_p}{1 + \theta^2 R_s/(2\varsigma\omega_n m)}, C_p + \frac{\theta^2}{m\omega_n^2}\right\}.
\tag{43}
$$

Then, we have

$$
C_s > C_p + \frac{\theta^2}{m\omega_n^2}.
\tag{44}
$$

2.　Negative capacitance in parallel with positive resistance

For the negative capacitance in parallel with resistance case, when $R \to \infty$, the characteristic function is as follows:

$$
a_3 s^3 + a_2 s^2 + a_1 s + a_0 = 0,
\tag{45}
$$

$$
\begin{aligned}
a_3 &= R_s\left(C_p - C_s\right) \\
a_2 &= 2\varsigma\omega_n R_s\left(C_p - C_s\right) + 1 \\
a_1 &= 2\varsigma\omega_n + \omega_n^2 R_s\left(C_p - C_s\right) + \frac{\theta^2 R_s}{m} \\
a_0 &= \omega_n^2
\end{aligned}
\tag{46}
$$

$$
\begin{array}{c|cc}
s^3 & a_3 & a_1 \\
s^2 & a_2 & a_0 \\
s^1 & b_1 & 0 \\
s^0 & a_0 & 0
\end{array}
\tag{47}
$$

Thus, the system should meet the following conditions:

$$
2\varsigma\omega_n R_s\left(C_p - C_s\right) + 1 > 0
$$
$$
\frac{\left[2\varsigma\omega_n R_s\left(C_p - C_s\right) + 1\right]\left[2\varsigma\omega_n + \omega_n^2 R_s\left(C_p - C_s\right) + \frac{\theta^2 R_s}{m}\right] - \omega_n^2 R_s\left(C_p - C_s\right)}{2\varsigma\omega_n R_s\left(C_p - C_s\right) + 1} > 0 \tag{48}
$$

Then, we get

$$
C_s < C_p + \frac{\varsigma}{\omega_n R_s} + \frac{\theta^2}{2m\omega_n^2} - \frac{\left\{\left[\left(2\varsigma\omega_n\right) + \frac{\theta^2 R_s}{m}\right]^2 - \left(\omega_n^2 + \omega_n\frac{\theta^2 R_s}{2\varsigma m}\right)\right\}^{0.5}}{2\omega_n^2 R_s}. \tag{49}
$$

3. Negative inductance and negative capacitance in series with resistance

When $\Gamma_R = 1$, the characteristic function can be written as

$$
s^2\left(C_p - C_s + L_s C_s/m\right) + \left(2\varsigma\omega_n C_p - C_s - \theta^2 R_s C_s/m\right)s + \omega_n^2\left(C_p - \theta^2/m - C_s\right) = 0. \tag{50}
$$

When $C_p < C_s$, according to the Routh–Hurwitz criterion, we have the following criterion:

$$
C_s < \min\left(C_p + L_s C_s/m, 2\varsigma\omega_n C_p - \theta^2 R_s C_s/m, C_p - \theta^2/m\right). \tag{51}
$$

Therefore, C_s should meet the following condition:

$$
C_s < C_p - \theta^2/m. \tag{52}
$$

When $C_p > C_s$, with the same process, it can be found that

$$
C_s > C_p + L_s C_s/m. \tag{53}
$$

3.2.2. Root Locus Analysis

We already discussed the stability of the controlled stiffness system according to the Routh–Hurwitz criterion, where some assumptions and simplifications were made to obtain the final limitation expressions of C_s. However, this cannot present the whole picture of the influence of shunt parameters. This section discusses the stability of the system with the root locus method.

1. Negative capacitance C_s

This subsection analyzes the root locus of the piezoelectric stack transducer with respect to the negative capacitance C_s for the three hybrid shunts. Firstly, the characteristic equation was written in form of the root locus form, allowing an easy simulation with MATLAB.

*   Negative capacitance in series with resistance shunt:

$$
1 - \frac{C_s\left[mR_s C_p s^3 + \left(m + R_s C_p c\right)s^2 + \left(c + kR_s C_p + \theta^2 R_s\right)s + k\right]}{mC_p s^2 + cC_p s + \left(\theta^2 + kC_p\right)} = 0. \tag{54}
$$

*   Negative capacitance in parallel with resistance shunt:

$$
1 + \left(C_p - C_s\right)\frac{mR_s s^3 + cR_s s^2 + kR_s s}{ms^2 + \left(c + \theta^2 R_s\right)s + k} = 0. \tag{55}
$$

- Negative inductance/negative resistance in series with resistance shunt:

$$1 + C_s \frac{L_s C_p m s^4 + (L_s C_p c - R_s C_p m)s^3 + (\theta^2 L_s + L_s C_p k - m - R_s C_p c)s^2 - (c + \theta^2 R_s + R_s C_p k)s - k}{m C_p s^2 + c C_p s + k C_p + \theta^2} = 0. \tag{56}$$

The root locus of the system with respect to C_s was analyzed graphically to evaluate the stability of the system. Figures 9 and 10 present the root locus of the piezoelectric stack transducer with respect to C_s for the negative capacitance in series with R_s and in parallel with R_s cases, respectively. It can be found that the system is stable when C_s is within [0.1, 5] µF. The damping improves with the increase of R_s. An optimal C_s can be found on the root locus curve. The results also imply that the negative capacitance in parallel with R_s case has a relatively better damping performance than the negative capacitance in series with R_s case. The hybrid negative-capacitance shunts can enhance stability when C_s is selected carefully.
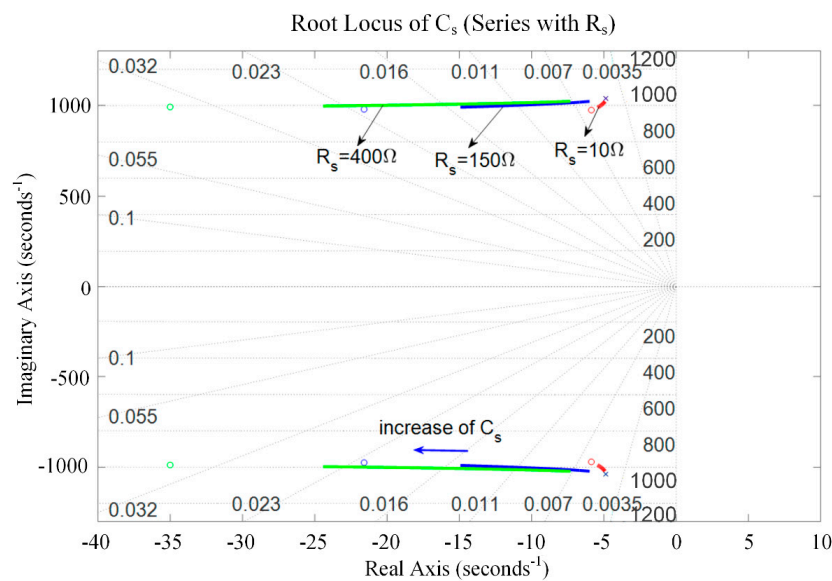

Figure 9. Root locus of the piezoelectric stack transducer with respect to C_s for the negative capacitance in series with R_s.
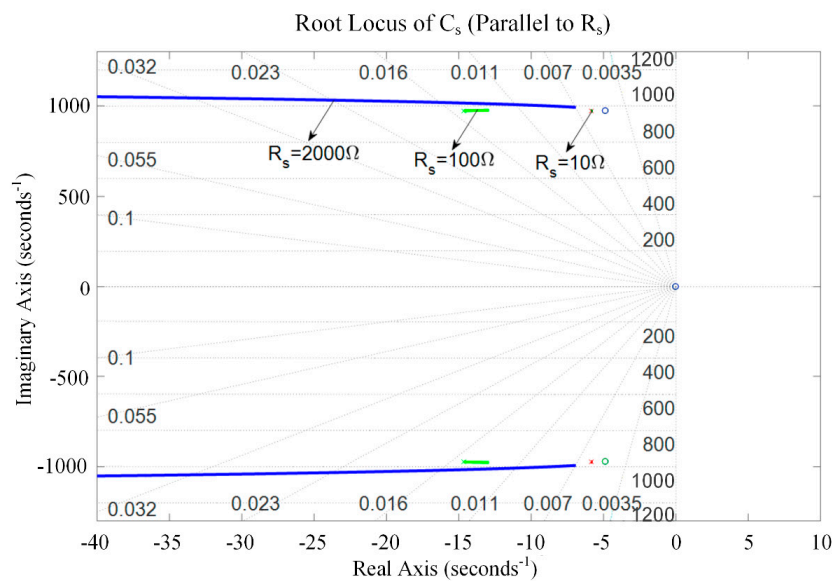

Figure 10. Root locus of the piezoelectric stack transducer with respect to C_s for the negative capacitance in parallel with R_s.

Figure 11 presents the root locus of the piezoelectric stack transducer with respect to C_s for the negative inductance/negative capacitance in series with resistance when $L_s = 10$ mH and $R_s = 50$ Ω. From Equation (56), it can be found that s → ∞ and C_s → ∞ leads the system to be unstable. When s → 0, we have C_s → ∞. Then, the root lies in the real axis. If C_s is used carefully, the system can also be kept stable. In this case, relatively considerable damping can be achieved.
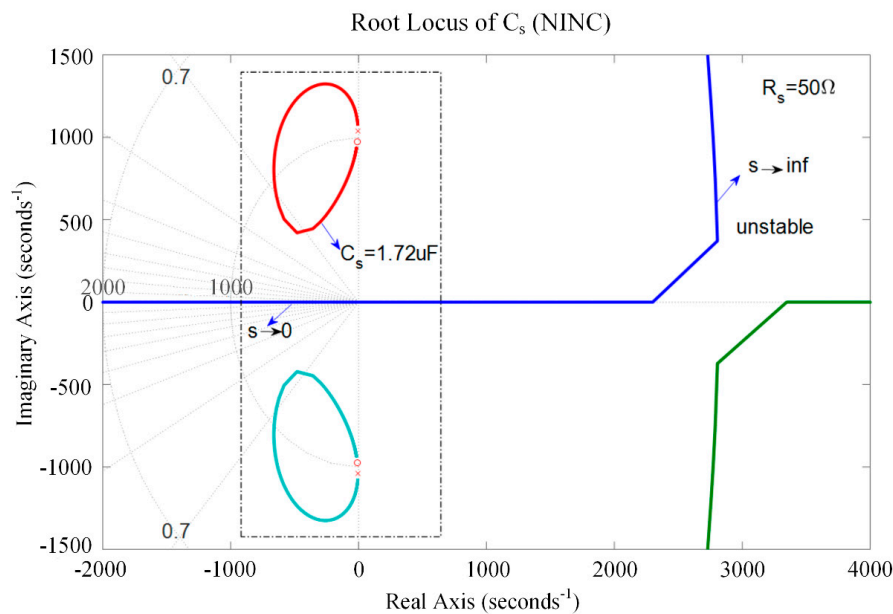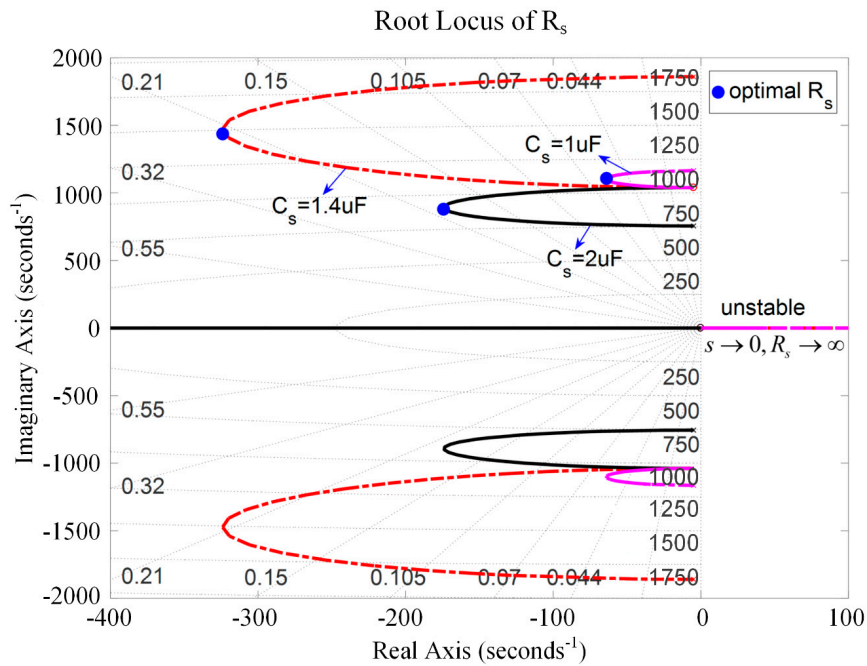

Figure 11. Root locus of the piezoelectric stack transducer with respect to C_s for the negative inductance/negative resistance in series with resistance shunt when $L_s = 10$ mH and $R_s = 50$ Ω.

2. Adjustable Resistance R_s

This subsection analyzes the root locus of the piezoelectric stack transducer with respect to the adjustable resistance R_s for the three hybrid shunts. The characteristic equation is also written in the root locus form.

- Negative capacitance in series with resistance R_s:

$$1 - R_s \frac{mC_sC_ps^3 + cC_sC_ps^2 + \left(\theta^2 C_s + kC_sC_p\right)s}{m\left(C_p - C_s\right)s^2 + c\left(C_p - C_s\right)s + \theta^2 + \left(C_p - C_s\right)k} = 0. \tag{57}$$

- Negative capacitance in parallel with resistance R_s:

$$1 + R_s \frac{m\left(C_p - C_s\right)s^3 + c\left(C_p - C_s\right)s^2 + \left[\theta^2 + k\left(C_p - C_s\right)\right]s}{ms^2 + cs + k} = 0. \tag{58}$$

- Negative inductance/negative resistance in series with resistance R_s:

$$1 - \frac{R_s\left(C_pC_sms^3 + C_pC_scs^2 + \left(\theta^2 + C_pk\right)C_ss\right)}{L_sC_pC_sms^4 + L_sC_pC_scs^3 + \left(\theta^2 L_sC_s + L_sC_sC_pk + mC_p - C_sm\right)s^2 + \left(C_p - C_s\right)cs + \left(C_p - C_s\right)k + \theta^2} = 0. \tag{59}$$

Equations (57) and (58) demonstrate that $s \to \infty$ results in $R_s \to \infty$. The root lies in the real axis. Figures 12 and 13 show the root locus of the system with respect to R_s for negative capacitance in series with R_s and in parallel with R_s, respectively. The results prove the correctness of the theoretical model. In this case, some roots are positive, which makes the system unstable. In other ranges, the system

can maintain stability with the change of C_s (C_s = 1 μF, 1.4 μF, and 2 μF). When C_s = 1.4 μF, we get a considerable damping performance, and the corresponding optimal R_s can also be found in Figures 12 and 13. Moreover, the parallel R_s case has relatively good damping performance compared to the series R_s case. Figure 14 is the root locus of the system with respect to the negative inductance/negative capacitance when C_s = 1.4 μF and 2 μF. The result shows that the system is conditionally stable with the change of R_s. One should carefully choose R_s, C_s, and L_s.

Figure 12. Root locus of the piezoelectric stack transducer with respect to R_s for the negative capacitance in series with R_s.
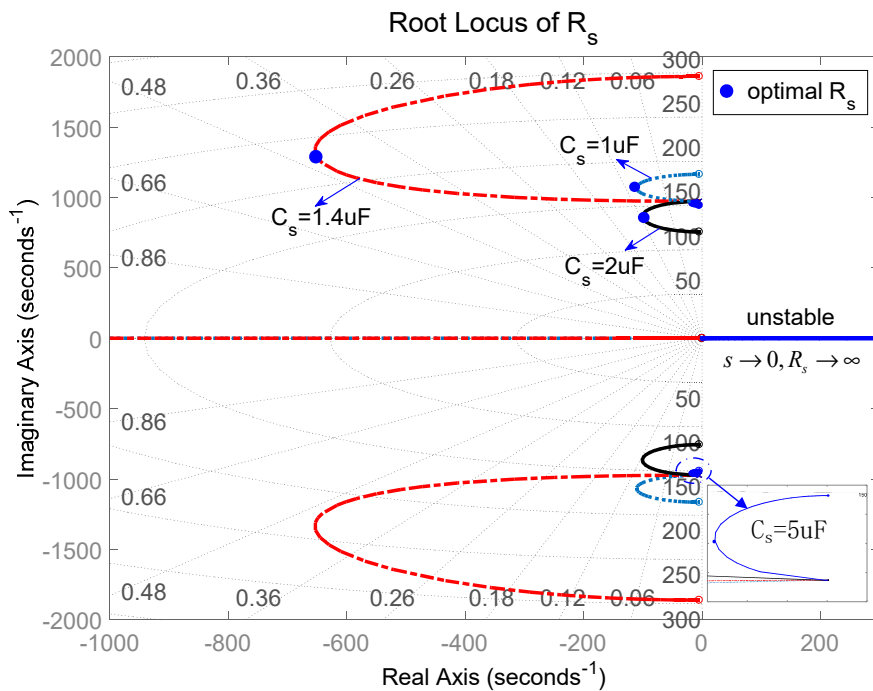

Figure 13. Root locus of the piezoelectric stack transducer with respect to R_s for the negative capacitance in parallel with R_s.
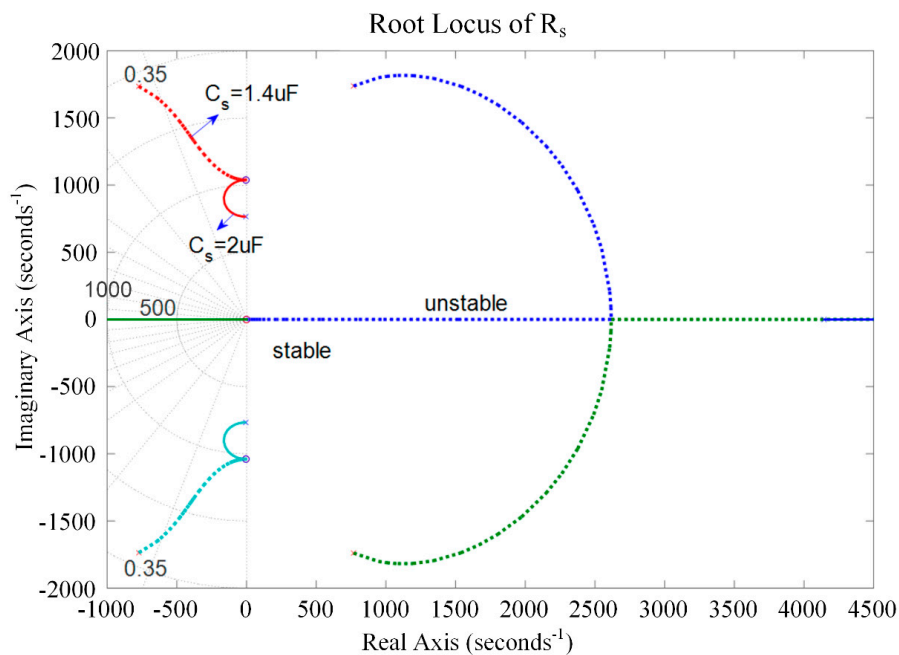
Figure 14. Root locus of the piezoelectric stack transducer with respect to R_s for the negative inductance/negative resistance in series with R_s.

3.3. Frequency Response Analysis

3.3.1. Piezoelectric Shunt Stiffness

As shown in the theoretical analysis of the PSS and PSD effects in the negative-impedance shunted piezoelectric stack transducer, all three hybrid shunts can achieve the controlled stiffness performance. The frequency response of the system was determined in order to further discuss the influence of PSS and PSD on the vibration control performance.

Figure 15 represents the frequency response of the piezoelectric stack transducer for the negative capacitance in series with R_s case. It can be found that the PSS is positive, which increases the natural frequency of the transducer when $C_s = 1.4$ μF. When $R_s = 10$ kΩ, the amplitude approximates to the uncontrolled condition. With the decrease of R_s, the amplitude decreases while the natural frequency increases. When $C_s = 2$ μF, this hybrid shunt can produce the negative stiffness effect, and the natural frequency of the system also decreases. In this case, the amplitude decreases with the increase of R_s. The corresponding optimal R_s can be found from Figure 12. The damping performance of PSD is shown in Table 2; it can be seen that PSD can achieve wonderful damping performance compared with the traditional pure resistive shunt method.

Table 2. Comparison of damping ratio shown in Figure 15.

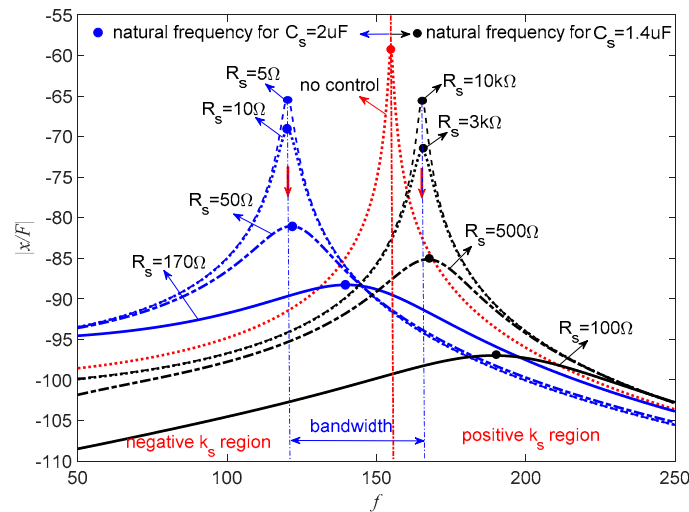| Negative Capacitance	Adjustable Resistance	Damping Ratio, ζ
Resistive load	$R_s = 100$ Ω	0.005
$C_s = 2$ μF	$R_s = 5$ Ω	0.0706
	$R_s = 10$ Ω	0.0973
	$R_s = 50$ Ω	0.2553
	$R_s = 170$ Ω	0.4721
$C_s = 1.4$ μF	$R_s = 10$ kΩ	0.0381
	$R_s = 3$ kΩ	0.0648
	$R_s = 500$ Ω	0.1684
	$R_s = 100$ Ω	0.26

Figure 15. Frequency response of the piezoelectric stack transducer with negative capacitance in series with R_s.

As suggested in Figure 7, the PSS is sensitive to R_s when $C_s = 1.4\ \mu\text{F}$. $C_s = 1\ \mu\text{F}$ is a better choice. Figure 16 shows the corresponding frequency response of the piezoelectric stack transducer in parallel with R_s with the change of C_s and R_s. When $C_s = 1\ \mu\text{F}$, the natural frequency increases, which means PSS is positive for $C_p > C_s$, and the amplitude decreases with the decrease of R_s. When $C_s = 2\ \mu\text{F}$, the natural frequency decreases, which indicates that PSS is negative for $C_p < C_s$, and the amplitude decreases with the increase of R_s. The amplitude of the transducer can be controlled by the change of R_s.
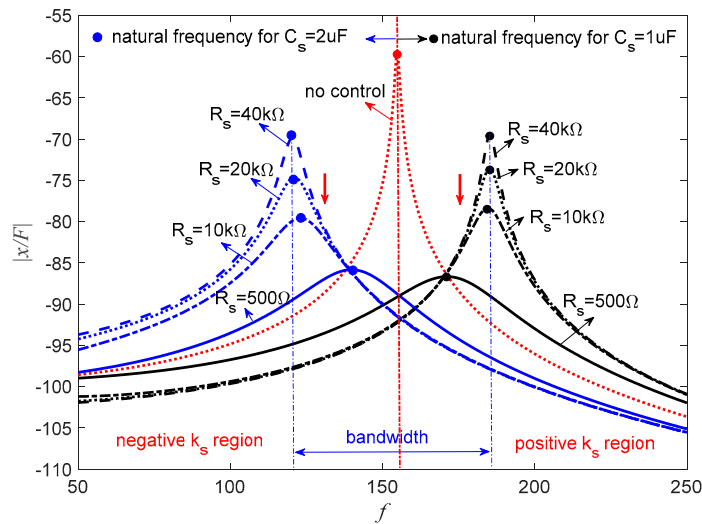

Figure 16. Frequency response of the piezoelectric stack transducer with negative capacitance in parallel with R_s.

Figure 17 represents the frequency response of the piezoelectric stack transducer with negative inductance/negative capacitance in series with R_s when $L_s = 10\ \text{mH}$. When $C_s = 1\ \mu\text{F}$, the natural frequency increases, which means the PSS is positive. The amplitude decreases with the decrease of R_s. While $C_s = 2\ \mu\text{F}$, the natural frequency decreases, which means the PSS is negative, and the amplitude decreases with the increase of R_s.
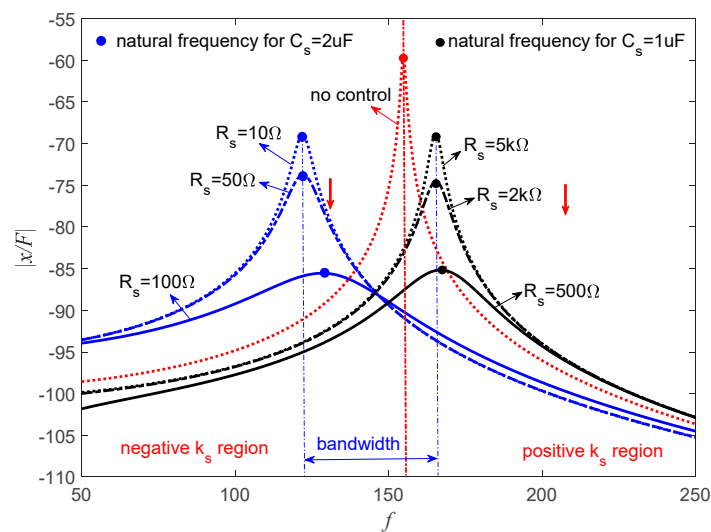
Figure 17. Frequency response of the piezoelectric stack transducer with negative inductance/negative capacitance in series with R_s when $L_s = 10$ mH.

This implies that R_s can be carefully selected to increase the damping of the system without changing the stiffness of the system, which is important in some special applications. Figures 15–17 also indicate that the bandwidth performance of the negative capacitance in parallel with R_s shunt is better than the other two cases, which can provide considerable controlled stiffness performance. If this transducer is used as an isolator, negative stiffness is a better choice. If one just wants to avoid the resonance of the system, both positive and negative stiffness are acceptable. The previous study by Heuss et al. [52] utilized different combinations of resistant, resonant, and negative capacitance to achieve the tuning of a vibration absorber. The tuning frequency band can be 120 Hz. We can also achieve this performance if negative capacitance and adjusting resistance are carefully designed.

3.3.2. Low-Frequency Vibration Control

Figure 18 shows the time history response of the transducer under sweep sine excitation when *Cs* is 1.4 μF. When R_s is 1 kΩ, only the response near the resonance is controlled. When R_s increases to 10 kΩ, the natural frequency increases. The response decreases dramatically near the resonance. Furthermore, the low-frequency vibration is also suppressed, and the bandwidth can reach up to 150 Hz. In view of vibration isolation, low-natural-frequency isolators can achieve bandwidth isolation performance when the excitation frequency is bigger than $\sqrt{2}\omega_n$, such as nonlinear vibration isolators [56–58], quasi-zero isolators [59,60], etc. These nonlinear vibration isolators can achieve broadband vibration isolation performance with negative dynamic stiffness of nonlinear isolators; however, the vibration suppression in the resonance region is dependent on damping. The proposed PSS can semi-actively decrease the stiffness of linear isolators to improve the vibration performance; therefore, it has application potential in isolation engineering. Furthermore, the PSS can also increase the stiffness of isolators to enhance the vibration suppression performance in the resonance region.
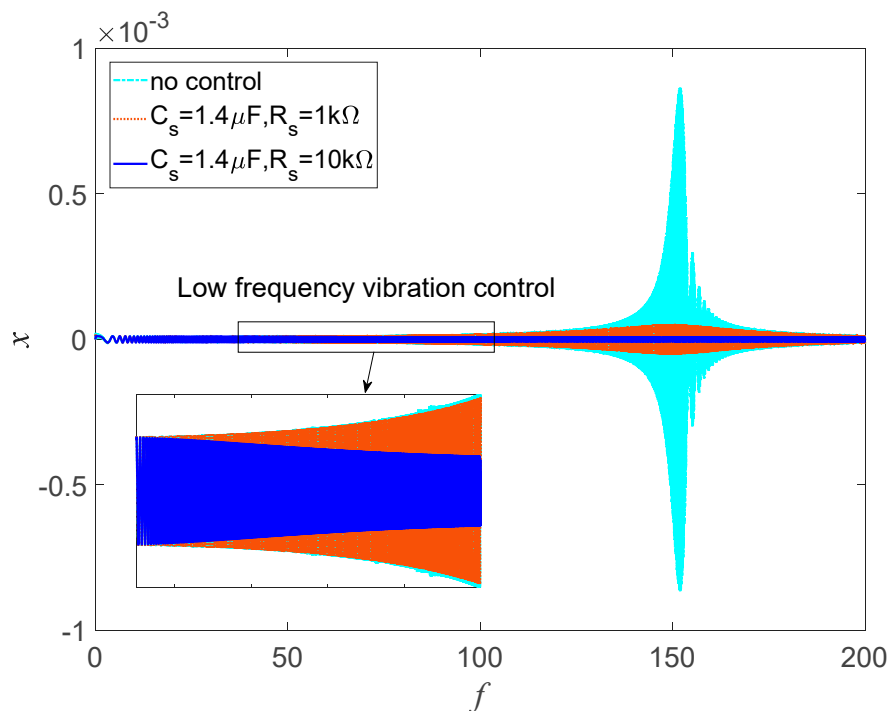
Figure 18. Time history response of the transducer under sweep sine excitation.

4. Conclusions

In this study, we proposed the novel controlled stiffness performance of a rhombic piezoelectric stack transducer with hybrid negative-impedance shunts. The governing equation of the transducer was established according to Lagrange's equation. Piezoelectric shunt stiffness and piezoelectric shunt damping were defined to analyze the stiffness and damping effects of transducer with three kinds of hybrid shunts. The Routh–Hurwitz criterion was employed to get the theoretical selection of negative capacitance. The root locus method was utilized to graphically judge the stability of the proposed three kinds of hybrid shunts. The results demonstrate that the piezoelectric stack transducer can produce both the stiffness and damping effects with hybrid shunts. With the change of negative capacitance, both negative and positive stiffness can also be obtained. Moreover, the negative stiffness effect requires a careful choice of the negative capacitance to sustain the stability of the system. Furthermore, negative capacitance in parallel with resistance demonstrated a considerably better stiffness bandwidth and damping performance than the other two shunts. The proposed PSS can be used to decrease the stiffness to decrease the natural frequency and, thus, to increase the vibration isolation band of linear or nonlinear isolators. Additionally, the PSS can be also used to adjust the stiffness to avoid resonance when the host structure is subjected to harmonic excitations. Future research may focus on experimental investigations of the PSS.

Author Contributions: Conceptualization, C.W.; methodology, L.H.; software, C.Z. and W.Z.; formal analysis, L.H.; resources, W.Z.; writing—original draft preparation, L.H.; writing—review and editing, C.W. and L.H.; visualization, C.Z.; writing—review and editing, C.W.

References

1. Marneffe, B.D.; Preumont, A. Vibration damping with negative capacitance shunts: Theory and experiment. *Smart Mater. Struct.* **2008**, *17*, 035015. [CrossRef]

2. Ji, H.; Qiu, J.; Badel, A.; Zhu, K. Semi-active Vibration Control of a Composite Beam using an Adaptive SSDV Approach. *J. Intell. Mater. Syst. Struct.* **2009**, *20*, 401–412.

3. Ji, H.; Qiu, J.; Zhu, K.; Chen, Y.; Badel, A. Multi-modal vibration control using a synchronized switch based on a displacement switching threshold. *Smart Mater. Struct.* **2009**, *18*, 035016. [CrossRef]

4. Zhou, S.; Cao, J.; Lin, J. Theoretical analysis and experimental verification for improving energy harvesting performance of nonlinear monostable energy harvesters. *Nonlinear Dyn.* **2016**, *86*, 1599–1611. [CrossRef]

5. Yan, B.; Zhou, S.; Litak, G. Nonlinear Analysis of the Tristable Energy Harvester with a Resonant Circuit for Performance Enhancement. *Int. J. Bifurcat. Chaos* **2018**, *28*, 1850092. [CrossRef]

6. Tao, K.; Tang, L.; Wu, J.; Lye, S.W.; Chang, H.; Miao, J. Investigation of Multimodal Electret-Based MEMS Energy Harvester with Impact-Induced Nonlinearity. *J. Microelectromech. Syst.* **2018**, *27*, 276–288. [CrossRef]

7. Zhou, S.; Zuo, L. Nonlinear dynamic analysis of asymmetric tristable energy harvesters for enhanced energy harvesting. *Commun. Nonlinear Sci. Numer. Simul.* **2018**, *61*, 271–284. [CrossRef]

8. Erturk, A.; Inman, D.J. Base excitation problem for cantilevered structures and correction of the lumped-parameter electromechanical model. In *Piezoelectric Energy Harvesting*; John Wiley and Sons, Ltd.: Hoboken, NJ, USA, 2011.

9. Song, G.; Li, W.; Wang, B.; Ho, S.C.M. A Review of Rock Bolt Monitoring Using Smart Sensors. *Sensors* **2017**, *17*, 776. [CrossRef] [PubMed]

10. Song, G.; Li, H.; Gajic, B.; Zhou, W.; Chen, P.; Gu, H. Wind turbine blade health monitoring with piezoceramic-based wireless sensor network. *Int. J. Smart Nano Mater.* **2013**, *4*, 150–166. [CrossRef]

11. Forward, R.L. Electronic damping of vibrations in optical structures. *Appl. Opt.* **1979**, *18*, 690–697. [CrossRef]

12. Hagood, N.W.; Von Flotow, A. Damping of structural vibrations with piezoelectric materials and passive electrical networks. *J. Sound Vib.* **1991**, *146*, 243–268. [CrossRef]

13. Kim, J.; Ryu, Y.; Choi, S. New shunting parameter tuning method for piezoelectric damping based on measured electrical impedance. *Smart Mater. Struct.* **2000**, *9*, 868–877. [CrossRef]

14. Hogsberg, J.; Krenk, S. Calibration of piezoelectric RL shunts with explicit residual mode correction. *J. Sound Vib.* **2017**, *386*, 65–81. [CrossRef]

15. Gardonio, P.; Casagrande, D. Shunted piezoelectric patch vibration absorber on two-dimensional thin structures: Tuning considerations. *J. Sound Vib.* **2017**, *395*, 26–47. [CrossRef]

16. Hollkamp, J.J. Multimodal Passive Vibration Suppression with Piezoelectric Materials and Resonant Shunts. *J. Intell. Mater. Syst. Struct.* **1994**, *5*, 49–57. [CrossRef]

17. Wu, S.-Y. Method for Multiple Mode Piezoelectric Shunting with Single PZT Transducer for Vibration Control. *J. Intell. Mater. Syst. Struct.* **1998**, *9*, 991–998. [CrossRef]

18. Behrens, S.; Moheimani, S.O.R.; Fleming, A.J. Multiple mode current flowing passive piezoelectric shunt controller. *J. Sound Vib.* **2003**, *266*, 929–942. [CrossRef]

19. Fleming, A.J.; Behrens, S.; Moheimani, S.O.R. Reducing the inductance requirements of piezoelectric shunt damping systems. *Smart Mater. Struct.* **2003**, *12*, 57–64. [CrossRef]

20. Choi, S.-B.; Kim, H.S.; Park, J.-S. Multi-mode vibration reduction of a CD-ROM drive base using a piezoelectric shunt circuit. *J. Sound Vib.* **2007**, *300*, 160–175. [CrossRef]

21. Lim, S.C.; Choi, S.B. Vibration control of an HDD disk-spindle system utilizing piezoelectric bimorph shunt damping: I. Dynamic analysis and modeling of the shunted drive. *Smart Mater. Struct.* **2007**, *16*, 891–900. [CrossRef]

22. Lim, S.C.; Choi, S.B. Vibration control of an HDD disk-spindle system using piezoelectric bimorph shunt damping: II. Optimal design and shunt damping implementation. *Smart Mater. Struct.* **2007**, *16*, 901–908. [CrossRef]

23. Sun, H.; Yang, Z.; Li, K.; Li, B.; Xie, J.; Wu, D.; Zhang, L. Vibration suppression of a hard disk driver actuator arm using piezoelectric shunt damping with a topology-optimized PZT transducer. *Smart Mater. Struct.* **2009**, *18*, 065010. [CrossRef]

24. Casagrande, D.; Gardonio, P.; Zilletti, M. Smart panel with time-varying shunted piezoelectric patch absorbers for broadband vibration control. *J. Sound Vib.* **2017**, *400*, 288–304. [CrossRef]

25. Yigit, U.; Cigeroglu, E.; Budak, E. Chatter reduction in boring process by using piezoelectric shunt damping with experimental verification. *Mech. Syst. Signal Process.* **2017**, *94*, 312–321. [CrossRef]

26. Liao, Y.; Sodano, H.A. Piezoelectric damping of resistively shunted beams and optimal parameters for maximum damping. *J. Vib. Acoust.* **2010**, *132*, 041014. [CrossRef]

27. Soltani, P.; Kerschen, G.; Tondreau, G.; Deraemaeker, A. Piezoelectric vibration damping using resonant shunt circuits: An exact solution. *Smart Mater. Struct.* **2014**, *23*, 125014. [CrossRef]

28. Berardengo, M.; Manzoni, S.; Conti, A.M. Multi-mode passive piezoelectric shunt damping by means of matrix inequalities. *J. Sound Vib.* **2017**, *405*, 287–305. [CrossRef]

29. Hogsberg, J.; Krenk, S. Balanced calibration of resonant shunt circuits for piezoelectric vibration control. *J. Intell. Mater. Syst. Struct.* **2012**, *23*, 1937–1948. [CrossRef]

30. Wang, W.; Hua, X.; Wang, X.; Chen, Z.; Song, G. Optimum design of a novel pounding tuned mass damper under harmonic excitation. *Smart Mater. Struct.* **2017**, *26*, 055024. [CrossRef]

31. Dominik, N.; Andrew, F.; Moheimani, S.O.R.; Manfred, M. Adaptive multi-mode resonant piezoelectric shunt damping. *Smart Mater. Struct.* **2004**, *13*, 1025–1035.

32. Bao, B.; Guyomar, D.; Lallart, M. Vibration reduction for smart periodic structures via periodic piezoelectric arrays with nonlinear interleaved-switched electronic networks. *Mech. Syst. Signal Process.* **2017**, *82*, 230–259. [CrossRef]

33. Ji, H.; Qiu, J.; Cheng, J.; Inman, D. Application of a Negative Capacitance Circuit in Synchronized Switch Damping Techniques for Vibration Suppression. *J. Vib. Acoust.* **2011**, *133*, 041015. [CrossRef]

34. Fleming, A.J.; Moheimani, S.O.R. Control orientated synthesis of high-performance piezoelectric shunt impedances for structural vibration control. *IEEE Trans. Control Syst. Technol.* **2005**, *13*, 98–112. [CrossRef]

35. Behrens, S.; Fleming, A.J.; Moheimani, S.O.R. A broadband controller for shunt piezoelectric damping of structural vibration. *Smart Mater. Struct.* **2003**, *12*, 18–28. [CrossRef]

36. Yan, B.; Zhang, X.; Niu, H. Design and test of a novel isolator with negative resistance electromagnetic shunt damping. *Smart Mater. Struct.* **2012**, *21*, 035003. [CrossRef]

37. Yan, B.; Zhang, X.; Luo, Y.; Zhang, Z.; Xie, S.; Zhang, Y. Negative impedance shunted electromagnetic absorber for broadband absorbing: Experimental investigation. *Smart Mater. Struct.* **2014**, *23*, 125044. [CrossRef]

38. Yan, B.; Wang, K.; Kang, C.-X.; Zhang, X.-N.; Wu, C.-Y. Self-Sensing Electromagnetic Transducer for Vibration Control of Space Antenna Reflector. *IEEE ASME Trans. Mechatron.* **2017**, *22*, 1944–1951. [CrossRef]

39. Stabile, A.; Aglietti, G.S.; Richardson, G.; Smet, G. Design and verification of a negative resistance electromagnetic shunt damper for spacecraft micro-vibration. *J. Sound Vib.* **2017**, *386*, 38–49. [CrossRef]

40. Zhang, Y.; Chan, Y.-J.; Huang, L. Thin broadband noise absorption through acoustic reactance control by electro-mechanical coupling without sensor. *J. Acoust. Soc. Am.* **2014**, *135*, 2738–2745. [CrossRef]

41. Neubauer, M.; Oleskiewicz, R.; Popp, K.; Krzyzynski, T. Optimization of damping and absorbing performance of shunted piezo elements utilizing negative capacitance. *J. Sound Vib.* **2006**, *298*, 84–107. [CrossRef]

42. Manzoni, S.; Moschini, S.; Redaelli, M.; Vanali, M. Vibration attenuation by means of piezoelectric transducer shunted to synthetic negative capacitance. *J. Sound Vib.* **2012**, *331*, 4644–4657. [CrossRef]

43. Beck, B.S.; Cunefare, K.A.; Collet, M. The power output and efficiency of a negative capacitance shunt for vibration control of a flexural system. *Smart Mater. Struct.* **2013**, *22*, 065009. [CrossRef]

44. Han, X.; Neubauer, M.; Wallaschek, J. Improved piezoelectric switch shunt damping technique using negative capacitance. *J. Sound Vib.* **2013**, *332*, 7–16. [CrossRef]

45. Neubauer, M.; Wallaschek, J. Vibration damping with shunted piezoceramics: Fundamentals and technical applications. *Mech. Syst. Signal Process.* **2013**, *36*, 36–52. [CrossRef]

46. Gripp, J.A.B.; Goes, L.C.S.; Heuss, O.; Scinocca, F. An adaptive piezoelectric vibration absorber enhanced by a negative capacitance applied to a shell structure. *Smart Mater. Struct.* **2015**, *24*, 125017. [CrossRef]

47. Pohl, M. An adaptive negative capacitance circuit for enhanced performance and robustness of piezoelectric shunt damping. *J. Intell. Mater. Syst. Struct.* **2017**, *28*, 2633–2650. [CrossRef]

48. Yan, B.; Wang, K.; Hu, Z.; Wu, C.; Zhang, X. Shunt damping vibration control technology: A review. *Appl. Sci.* **2017**, *7*, 494. [CrossRef]

49. Pohl, M.; Rose, M. Piezoelectric shunt damping of a circular saw blade with autonomous power supply for noise and vibration reduction. *J. Sound Vib.* **2016**, *361*, 20–31. [CrossRef]

50. Vaclavik, J.; Kodejska, M.; Mokry, P. Wall-plug efficiency analysis of semi-active piezoelectric shunt damping systems. *J. Vib. Control* **2016**, *22*, 2582–2590. [CrossRef]

51. Preumont, A.; de Marneffe, B.; Deraemaeker, A.; Bossens, F. The damping of a truss structure with a piezoelectric transducer. *Comput. Struct.* **2008**, *86*, 227–239. [CrossRef]

52. Heuss, O.; Salloum, R.; Mayer, D.; Melz, T. Tuning of a vibration absorber with shunted piezoelectric transducers. *Arch. Appl. Mech.* **2016**, *86*, 1715–1732. [CrossRef]

53. Zheng, W.; Yan, B.; Ma, H.; Wang, R.; Jia, J.; Zhang, L.; Wu, C. Tuning of natural frequency with electromagnetic shunt mass. *Smart Mater. Struct.* **2019**, *28*, 25–26. [CrossRef]

54. Chen, J.; Zhang, C.; Xu, M.; Zi, Y.; Zhang, X. Rhombic micro-displacement amplifier for piezoelectric actuator and its linear and hybrid model. *Mech. Syst. Signal Process.* **2015**, *50*, 580–593. [CrossRef]

55. Yan, B.; Ma, H.; Zheng, W.; Jian, B.; Wang, K.; Wu, C. Nonlinear electromagnetic shunt damping for nonlinear vibration isolators. *IEEE ASME Trans. Mechatron.* **2019**. [CrossRef]

56. Ibrahim, R. Recent advances in nonlinear passive vibration isolators. *J. Sound Vib.* **2008**, *314*, 371–452. [CrossRef]

57. Yang, K.; Harne, R.; Wang, K.; Huang, H. Dynamic stabilization of a bistable suspension system attached to a flexible host structure for operational safety enhancement. *J. Sound Vib.* **2014**, *333*, 6651–6661. [CrossRef]

58. Yan, B.; Ma, H.; Zhao, C.; Wu, C.; Wang, K.; Wang, P. A vari-stiffness nonlinear isolator with magnetic effects: Theoretical modeling and experimental verification. *Int. J. Mech. Sci.* **2018**, *148*, 745–755. [CrossRef]

59. Carrella, A.; Brennan, M.; Waters, T. Static analysis of a passive vibration isolator with quasi-zero-stiffness characteristic. *J. Sound Vib.* **2007**, *301*, 678–689. [CrossRef]

60. Yan, B.; Ma, H.; Jian, B.; Wang, K.; Wu, C. Nonlinear dynamics analysis of a bi-state nonlinear vibration isolator with symmetric permanent magnets. *Nonlinear Dyn.* **2019**, 1–21. [CrossRef]